



Improved nitrogen retrievals with airborne-derived fluorescence and plant traits quantified from VNIR-SWIR hyperspectral imagery in the context of precision agriculture

Carlos Camino^a, Victoria González-Dugo^a, Pilar Hernández^a, J.C. Sillero^b, Pablo J. Zarco-Tejada^{a,*}

^a Instituto de Agricultura Sostenible (IAS), Consejo Superior de Investigaciones Científicas (CSIC), Alameda del Obispo s/n, 14004, Córdoba, Spain

^b Instituto Andaluz de Investigación y Formación Agraria, Pesquera, Alimentaria y de la Producción Ecológica (IFAPA), Centro Alameda del Obispo, s/n, 14004, Córdoba, Spain

ARTICLE INFO

Keywords:

Nitrogen concentration
Chlorophyll fluorescence
Chlorophyll content
NIR indices
Hyperspectral
Airborne

ABSTRACT

In semi-arid conditions, nitrogen (N) is the main limiting factor of crop yield after water, and its accurate quantification remains essential. Recent studies have demonstrated that solar-induced chlorophyll fluorescence (SIF) quantified from hyperspectral imagery is a reliable indicator of photosynthetic activity in the context of precision agriculture and for early stress detection purposes. The role of fluorescence might be critical to our understanding of N levels due to its link with photosynthesis and the maximum rate of carboxylation (V_{cmax}) under stress. The research presented here aimed to assess the contribution played by airborne-retrieved solar-induced chlorophyll fluorescence (SIF) to the retrieval of N under irrigated and rainfed Mediterranean conditions. The study was carried out at three field sites used for wheat phenotyping purposes in Southern Spain during the 2015 and 2016 growing seasons. Airborne campaigns acquired imagery with two hyperspectral cameras covering the 400–850 nm (20 cm resolution) and 950–1750 nm (50 cm resolution) spectral regions. The performance of multiple regression models built for N quantification with and without including the airborne-retrieved SIF was compared with the performance of models built with plant traits estimated by model inversion, and also with standard approaches based on single spectral indices. Results showed that the accuracy of the models for N retrieval increased when chlorophyll fluorescence was included ($r_{LOOCV}^2 \geq 0.92$; $p < 0.0005$) as compared to models only built with chlorophyll a + b (C_{ab}), dry matter (C_m) and equivalent water thickness (C_w) plant traits (r_{LOOCV}^2 ranged from 0.68 to 0.77; $p < 0.005$). Moreover, nitrogen indices (NIs) centered at 1510 nm yielded more reliable agreements with N concentration ($r^2 = 0.69$) than traditional chlorophyll indices (TCARI/OSAVI $r^2 = 0.45$) and structural indices (NDVI $r^2 = 0.57$) calculated in the VNIR region. This work demonstrates that under irrigated and non-irrigated conditions, indicators directly linked with photosynthesis such as chlorophyll fluorescence improves predictions of N concentration.

1. Introduction

Nitrogen (N) content plays an important role in the plant life cycle. In most situations, N is the major limiting factor of crop yield after water deficiency, and it is an essential element in plant growth (Lemaire et al., 2008). It is well documented that an adequate N supply is crucial for the maintenance of plant biochemistry quality (Nobel, 2009), and that N deficiency greatly changes the photosynthetic capacity, leading to a decrease in photosynthetic quantum yield and light-saturated photosynthetic rate (Khamis et al., 1990). N management of crops has important economic impacts and environmental implications, although

nitrogen overfertilization is widely used by farmers as a form of insurance against uncertain soil fertility (Tremblay et al., 2012). In particular, a higher N supply causes significant effects on the environment. Hence, an adequate N management strategy is needed to guide precision diagnosis of soil status and efficient crop management.

Traditionally, the N concentration is estimated using chemical analyses based on leaf tissue, such as Kjeldahl-digestion and Dumas-combustion, due to their reliability in organic N determination. However, these methods are destructive, time consuming, and need complex analysis. Moreover, traditional N estimates provide only limited information, as sampling is based on only a limited number of sites

* Corresponding author.

E-mail address: pablo.zarco@csic.es (P.J. Zarco-Tejada).

in a given field; they are therefore not suitable for the continuous monitoring of N content in the entire field. For these reasons, remote sensing and, in particular, hyperspectral imagery, can be useful for monitoring spatial and temporal variations in crop N content over large areas (Quemada et al., 2014).

The use of simple empirical models that incorporate hyperspectral reflectance indices is still the dominant method used to estimate N (Ferwerda et al., 2005; Stroppiana et al., 2009; Herrmann et al., 2010; Wang et al., 2012; Li et al., 2014; Mahajan et al., 2016). Several studies have shown improvements in canopy N quantifications using reflectance bands in the near infrared (NIR) and in the short-wave infrared (SWIR) regions (Kokaly, 1999; Ferwerda et al., 2005; Herrmann et al., 2010; Pimstein et al., 2011; Gnyp et al., 2014; Mahajan et al., 2014), especially when indices calculated from wavelengths centered at 850 and 1510 nm are used, as described in detail by Herrmann et al. (2010). Serrano et al. (2002) also showed that the combination of the 1510 nm and 1680 nm spectral regions was sensitive to N concentration in green biomass. Nevertheless, and despite the successful empirical relationships, nitrogen estimation at the canopy level from remote sensing requires appropriate modelling strategies due to the large contribution of structural and shadow effects to canopy reflectance (Zarco-Tejada et al., 2005). On the other hand, radiative transfer models offer advantages compared to index-based empirical models regarding robustness and transferability (Jacquemoud and Baret, 1990; Zarco-Tejada et al., 2004; Schlerf and Atzberger, 2006; Wang et al., 2015), and these have been widely proposed as a method for retrieving chlorophyll content, dry matter, and water content from remote sensing data (Clevers and Kooistra, 2012; Jacquemoud and Baret, 1990; Zarco-Tejada et al., 2004). In this context, recent studies have evaluated the estimation of leaf N content using models built with leaf and canopy biophysical parameters retrieved by inversion (e.g. Wang et al., 2015), and these have yielded reasonable success ($r^2 = 0.58$).

In recent years, the quantification of chlorophyll fluorescence has attracted increasing attention in the context of global monitoring of crop physiology and vegetation functioning, and this method can offer improvements on the estimation of N status (Tremblay et al., 2012). Chlorophyll fluorescence is generally considered as a direct proxy for electron transport rate and hence photosynthetic activity (Genty et al., 1989; Weis and Berry, 1987). The leaf-level maximum carboxylation rate (V_{cmax} ; $\mu\text{mol CO}_2 \text{ m}^{-2} \text{ s}^{-1}$) is closely related to the chlorophyll content at leaf scale (Croft et al., 2017; Houborg et al., 2013) and with solar-induced chlorophyll fluorescence (SIF) (Rascher et al., 2015; Yang et al., 2015). In this regard, SIF can be considered as a direct link with V_{cmax} through its strong connexion to chlorophyll content and photosynthetic activity (Walker et al., 2014). In fact, recent studies have demonstrated the link between chlorophyll fluorescence and photosynthetic activity at leaf and canopy levels (see e.g. Zarco-Tejada et al., 2013, 2016; Cendrero-Mateo et al., 2016). The rationale is based on the dependence of chlorophyll fluorescence emissions on chlorophyll concentration and photosystem I (PSI) and II (P_{siII}) efficiency (Lichtenthaler et al., 1996). It is well documented that N deficiency affects P_{siII} photochemistry, lowering the quantum yield electron transport, the photochemical efficiency, and therefore the assimilation rate (Lu and Zhang, 2000; Jin et al., 2015).

Crop water status may alter N balance: crop N demand is reduced under drought conditions, as growth rate diminishes (Gonzalez-Dugo et al., 2010). In arid and semi-arid environments, the co-limitation between nitrogen and water often reduces crop production which therefore must be considered together (Sadras, 2004). For these reasons, spectral indicators related to the leaf functioning, as chlorophyll fluorescence, is a potentially important candidate for improving the quantification of N concentration using passive remote sensing techniques. The present study aimed to explore the contribution of airborne-retrieved chlorophyll fluorescence to the quantification of N concentration using hyperspectral imagery. Specifically, we evaluated the fluorescence quantification in spring wheat (early sowing) grown

under rainfed and irrigated conditions to assess whether they contributed significantly to the retrieval of N concentration in the context of precision agriculture and plant phenotyping experiments.

2. Material and methods

2.1. Study area

The study was carried out in 2015 and 2016 at three field trial sites for durum wheat (*Triticum turgidum* L. var. *durum*) and bread wheat (*Triticum aestivum* L.) selection in Southern Spain. The sowing date for all sites was mid-November in the previous year. Regarding fertilization, pest and disease management, all the plots received the same treatment at all trial sites. Fertilization with diammonium phosphate and urea was carried out in early November, while similar amounts of fungicides and pesticides were applied at the early and middle growth stages at all trial sites.

The first trial site was located in Ecija (EC), near Seville, Southern Spain ($37^{\circ}32'17''\text{N}$, $5^{\circ}06'57''\text{W}$), which was managed under rainfed conditions in 2015. The experiment was designed with a balanced square lattice design using 300 individual plots (6×1.25 m) separated in four blocks, with 150 varieties of durum wheat and 150 of bread wheat. Each cultivar was replicated three times per block (Fig. 1a).

The second site trial was in Carmona (CA), also close to Seville, Southern Spain ($37^{\circ}30'29''\text{N}$, $5^{\circ}34'42''\text{W}$) in 2015. The experiment comprised 882 individual plots (7.5×1.25 m) divided into two blocks managed under rainfed conditions and one block under irrigated conditions. Each block contained a mixture of varieties of durum and bread wheat, each cultivar replicated three times per block (Fig. 1b).

The third trial site was managed by IFAPA in Santaella (SA), near Cordoba, Southern Spain ($37^{\circ}31'34''\text{N}$, $4^{\circ}50'40''\text{W}$) in 2016, where 20 varieties of durum wheat and 20 varieties of bread wheat were replicated three times under irrigated and rainfed conditions (Fig. 1c). The plot size was 15 m^2 (10×1.5 m).

2.2. Field data

In order to assess the physiology and the leaf optical properties of the wheat, a series of leaf-level measurements were made concurrently with the airborne flights at midday (12:00 to 13:00 h local time) at all the trial sites. A summary of field measurements and airborne campaigns at each trial site is shown in Table 1. The wheat growth stage during the flight campaigns refers to the stem length at the time of the first flight in Santaella (SA-1) and grain filling (milking stage) at the time of the flights in EC, CA and the second flight in Santaella (SA-2).

Leaf water potential (ψ_L ; MPa) was measured using a pressure chamber (Model 600 Pressure Chamber Instrument, PMI Instrument Company, Albany, NY, USA) on two sunlit leaves per plot. Assimilation rate (A ; $\mu\text{mol m}^{-2} \text{ s}^{-1}$) and stomatal conductance (G_s ; $\text{mmol m}^{-2} \text{ s}^{-1}$) were measured using a photosynthesis measurement system (LCDproSD, ADC Bioscientific Ltd., Herts, UK) on two sunlit leaves per plot. Steady-state leaf fluorescence yield (F_t) and a SPAD chlorophyll content indicator were measured on 10–15 leaves per plot using a FluorPen FP100 (Photon Systems Instruments, Brno, Czech Republic) and a chlorophyll meter (SPAD-502, Minolta Corp., Ramsey, NJ, USA), respectively. The relationship between chlorophyll concentration and SPAD readings for wheat found by Uddling et al. (2007) was applied to convert SPAD data into chlorophyll content ($\mu\text{g cm}^{-2}$). Total N concentration was determined by the Kjeldhal method (Kjeldahl, 1883) on 20–25 sunlit leaves sampled per plot. As in the rest of the physiological measurements, a random selection of the sunlit leaves was carried out from the central area of each plot.

2.3. Airborne hyperspectral imagery

A hyperspectral imager covering the visible and near-infrared

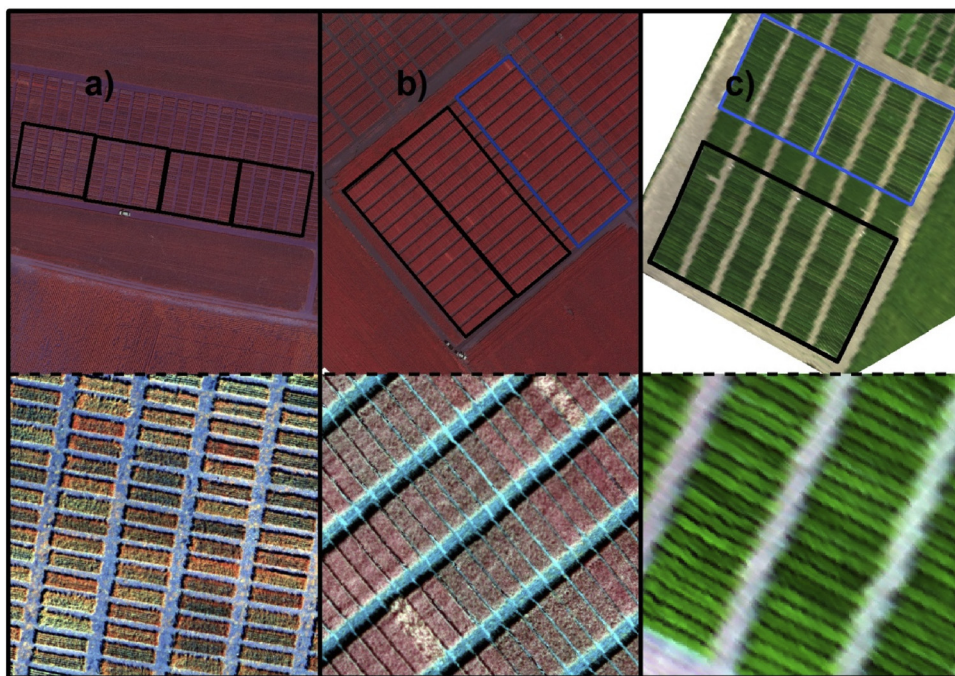


Fig. 1. Scene of the field trial sites at EC (a), CA (b) and Santaella (c) obtained with a color infrared camera (CIR; a and b, not used for analysis in this study) and the hyperspectral imagery (c) on board the aircraft. Black rectangles indicate plots under rainfed conditions and blue rectangles indicate plot under irrigated conditions. (For interpretation of the references to colour in this figure legend, the reader is referred to the web version of this article.)

Table 1
Field measurements and flight dates during the 2015 and 2016 campaigns.

| Year | Site | Flight dates | Type of flight ^a | Field measurements | Plots with field data |
|------|------|--------------|-----------------------------|-------------------------------|-------------------------------------|
| 2015 | EC | 28/05 | Noon (T + VNIR + SWIR) | ψ_L , A, Gs, Ft, SPAD, N | 12 ^b |
| | CA | 30/05 | Noon (T + VNIR + SWIR) | ψ_L , A, Gs, Ft, SPAD, N | 18 ^b |
| 2016 | SA-1 | 17/03 | Noon (T + VNIR + SWIR) | ψ_L , A, Gs, Ft, SPAD, N | 24 ^b and 45 ^c |
| | SA-2 | 26/04 | Noon (T + VNIR + SWIR) | ψ_L , A, Gs, Ft, SPAD, N | 24 ^b and 50 ^c |

^a T = thermal camera, VNIR = hyperspectral visible and infrared camera (400–885 nm), SWIR = hyperspectral near-infrared and short-wave infrared camera (950–1750 nm).

^b Number of plots with all leaf measurements.

^c Number of plots with only measurements of SPAD and total leaf nitrogen.

region (Micro-Hyperspec VNIR, Headwall Photonics, Fitchburg, MA, USA) and a second hyperspectral imager covering the NIR and the SWIR regions (Micro-Hyperspec NIR-100, Headwall Photonics) were installed in tandem on a Cessna aircraft operated by the Laboratory for Research Methods in Quantitative Remote Sensing (QuantaLab), Consejo Superior de Investigaciones Científicas (IAS-CSIC, Spain). Imagery was acquired at 250 m above ground level with the aircraft flying on the solar plane during the flight campaigns of 2015 and 2016. The campaigns were flown at midday (local time) to minimize differences due to sun angle effects between flights.

The micro-hyperspec VNIR was set up with a configuration of 260 spectral bands acquired at 8 nm/pixel and 12-bit radiometric resolution in the 400–885 nm spectral region, thus yielding a 6.4 nm Full Width at Half Maximum (FWHM) with a 25- μ m slit. The acquisition and storage module had a 50 fps frame rate with an integration time of 25 ms. The 8-mm focal length lens yielded an IFOV of 0.93 mrad and an angular FOV of 50° with a spatial resolution of 20 cm (Fig. 2a) (further information regarding the setup of micro-hyperspec VNIR can be obtained from Zarco-Tejada et al., 2016).

The micro-hyperspec NIR-100 camera was flown with a configuration of 165 spectral bands and 16-bit radiometric resolution in the

spectral region of 950–1750 nm, yielding 6.05 nm FWHM with a 25- μ m slit and an optical aperture of $f/1.4$. The FWHM and the center wavelength for each spectral band were derived after spectral calibration using a Cornerstone 260 1/4 m Monochromator (model 74100; Oriel Instruments, USA) and the XE-1 Xenon Calibration Light Source (Oceanic Optics, USA). The frame rate on board the aircraft was set to 50 fps with an integration time of 40 ms. The 12.5-mm focal length lens yielded an angular FOV of 38.6° with a spatial resolution of 60 cm (Fig. 2b).

Radiometric calibration of the hyperspectral cameras and *ortho*-rectification of the imagery were carried out as described by Zarco-Tejada et al. (2016). Atmospheric correction of the imagery was performed using aerosol optical depth (AOD) and weather data to simulate the incoming irradiance using the SMARTS model (Gueymard, 1995; Gueymard et al., 2002), measured in the field concurrently with the airborne flights. The SMARTS model has been used in previous studies to calculate reflectance from both multispectral and hyperspectral imagery (Berni et al., 2009; Zarco-Tejada et al., 2012, 2016; Calderón et al., 2013, 2015). A further step was carried out to apply an empirical line calibration (Smith and Milton, 1999) using field-measured spectra to remove noise. The average radiance and reflectance values of selected wheat plots from each trial site are shown in Fig. 3.

2.4. Fluorescence retrieval and calculation of narrow-band indices from the airborne hyperspectral imagery

The atmospheric O₂-A oxygen absorption band at 760.5 nm was used for the fluorescence retrieval via the *in-filling* method. In particular, the Solar Induced Fluorescence (SIF) was quantified from the radiance spectra (Fig. 3a) using the Fraunhofer Line Depth (FLD) principle (Plascyk and Gabriel, 1975) as described in Zarco-Tejada et al. (2013, 2016). The SIF signal calculated using the *in filling* method was based on two spectral bands *in* and *out* the O₂-A feature, as described in Meroni et al. (2010). The FLD2 method used L_{in} (L762 nm) in this study extracted the radiance and L_{out} (L750 nm) from the airborne imagery, and the irradiance E_{in} (E762 nm) and E_{out} (E750 nm) from irradiance spectra concurrently measured at the time of the flights. Measurements were made using an ASD Field Spectrometer (FieldSpec Handheld Pro, ASD Inc., CO, USA) with a cosine corrector-diffuser probe for the entire

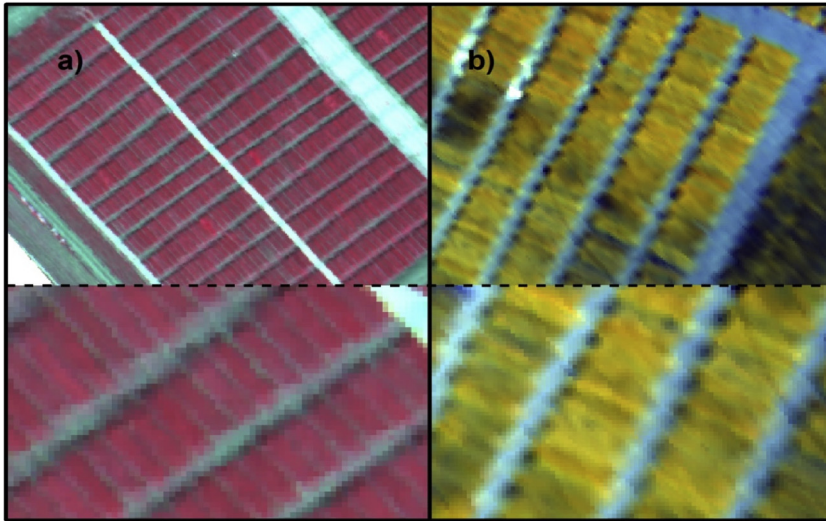


Fig. 2. Sample hyperspectral VNIR (400–800 nm region) (a) and hyperspectral NIR (900–1700 nm region) (b) imagery acquired during the 2015 and 2016 airborne campaigns performed at the trial sites at CA and SA-1, respectively. The central region of the plot was used to calculate hyperspectral indices and to quantify chlorophyll fluorescence.

400–1000 nm spectral region. A modelling study by Damm et al. (2011) quantified the effects of the spectral sampling interval, spectral resolution, signal to noise ratio (SNR) and the spectral shift on the accuracy of the fluorescence retrieval using the O_2-A feature. They demonstrated the feasibility of the SIF retrieval via the FLD methods with broader spectral bandwidths (i.e., 5–7 nm FWHM) when high spectral sampling (below 2.5 nm) and SNR higher than 300:1 were available. These results agree with the fluorescence retrievals shown in Zarco-Tejada et al. (2012) and later in Damm et al. (2015) with APEX. According to these works, the hyperspectral configuration used in this study is suitable for the SIF retrievals (1.85 nm sampling interval, 6.4 nm bandwidths and SNR of 300:1 with spatial binning).

Narrow-band indices were calculated from the average reflectance per plot using the 260 spectral bands acquired by the micro-hyperspec VNIR, and from the 164 spectral bands acquired by the micro-hyperspec NIR cameras (Fig. 3b). In the SWIR region, the atmospheric water absorption spectral region (1330–1490 nm) was masked before analysis. Table 2 groups the vegetation indices (VIs) calculated from the micro-hyperspec VNIR into four categories related to: 1) structure, 2) chlorophyll concentration, 3) chlorophyll fluorescence, and 4) nitrogen indices (NIs) using NIR and SWIR spectral domains.

2.5. Modelling methods

Radiative transfer simulations were carried out with PROSPECT (Jacquemoud and Baret, 1990) linked to the SAILH model (Baret et al.,

1992). Biophysical canopy parameters by means of numerical model inversion were estimated using look-up tables (LUT). The input variables and their ranges in PROSPECT and SAILH models are shown in Table 3. The viewing geometry, defined by the solar zenith and azimuth, and the viewing angles needed to simulate canopy reflectance were extracted for each flight date. In order to minimize the impact of the viewing geometry at each flight date and time, a step of five degrees around the solar zenith angle during the flights was applied to the PROSPECT-SAILH radiative transfer model inversions.

In this study two standard model inversions and one inversion method by steps were performed. The range of variation for C_{ab} was determined on the basis of prior field information. In the standard model inversion method, the chlorophyll a + b, water and dry matter content were estimated at the same time, while in the inversion method by steps, the estimation of biophysical canopy parameters required consecutive steps (e.g.; as in Wang et al., 2015). The spectral range between 400 and 800 nm measured with the micro-hyperspec VNIR camera was used in the standard model inversion method (named here as INV-1), while the entire spectral region (400–1700 nm) from both hyperspectral VNIR and NIR-100 cameras was used in the full-range inversion (here called INV-2) and in the inversion model by steps. In the inversion by steps, the main input parameters were calculated using specific spectral ranges where the biophysical parameters have the greatest influence on the reflectance and transmittance. The procedure was conducted as follows: 1) leaf angle distribution function (LADF) was estimated over the entire spectral domain (400–1750 nm) with

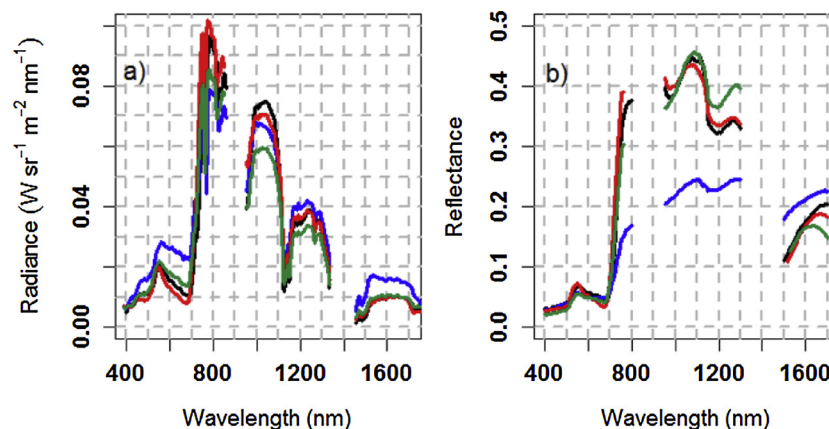


Fig. 3. Mean radiance in $W sr^{-1} m^{-2} nm^{-1}$ (a) and reflectance spectra (b) retrieved from hyperspectral cameras at EC (in blue), CA (in black), SA-1 (in red) and SA-2 (in Green). (For interpretation of the references to colour in this figure legend, the reader is referred to the web version of this article.)

Table 2
Summary of the vegetation indices using the VNIR (400–800 nm region) and NIR (900–1700 nm region) hyperspectral airborne imagery.

| Indices | Equation | Reference |
|---------------------------------------|--|--|
| Structural indices | | |
| Normalized Diff. Veg. Index | $NDVI = (R_{800}(R_{670})/(R_{800} + R_{670}))$ | Rouse et al. (1973) |
| Opt. Soil-Adjusted Veg. Index | $OSAVI = (1 + 0.16)(R_{800} - R_{670})/(R_{800} + R_{670} + 0.16)$ | Rondeaux et al. (1996) |
| Renormalized Diff. Veg. Index | $RDVI = (R_{800} - R_{670})/(R_{800} + R_{670})^{0.5}$ | Roujean and Breon (1995) |
| MCARI/MTVI2 | MCARI/MTVI2 | Eitel et al. (2007) |
| Chlorophyll a + b indices | | |
| Transf. Chl. Absorp. Rfl. Index | $TCARI = 3[(R_{700} - R_{670}) - 0.2 (R_{700} - R_{550})(R_{700}/R_{670})]$ | Haboudane et al. (2002) |
| TCARI/OSAVI | TCARI/OSAVI | Haboudane et al. (2002) |
| Mod. Chl. Absorp. Rfl. Index | $MCARI = [(R_{700} - R_{670}) - 0.2 (R_{700} - R_{550})](R_{700}/R_{670})$ | Daughtry (2000) |
| Pig. Spec. Simpl. Ratio Chl. b | $PSSRb = R_{800}/R_{635}$ | Blackburn (1998) |
| Gitelson and Merzlyak Indices | $GM1 = R_{750}/R_{550}$; $GM2 = R_{750}/R_{700}$ | Gitelson and Merzlyak (1997) |
| Vogelmann Index | $VOG = R_{740}/R_{720}$ | Vogelmann et al. (1993) |
| Red-edge CI | $CI = R_{750}/R_{710}$ | Zarco-Tejada et al. (2001) |
| Chlorophyll fluorescence (SIF) | | |
| SIF | $FLD2 = d - Rb$; where $d = L_{762}$; $R = (L_{762} - L_{750})/(E_{762} - E_{750})$ and $b = E_{762}$ | Moya et al. (2004); Plascyk and Gabriel (1975) |
| Nitrogen indices (NIs) | | |
| Double-peak C. N | $DCNI = (R_{720} - R_{700})(R_{700}R_{670})/(R_{720} - R_{670}) + 0.3$ | Chen et al., 2010 |
| TCARI _{1510nm} | $TCARI_{1510} = 3[(R_{700} - R_{1510}) - 0.2 (R_{700} - R_{550})](R_{700}/R_{1510})$ | Herrmann et al., 2010 |
| TCARI/OSAVI _{1510nm} | $TCARI_{1510}/OSAVI_{1510} = TCARI_{1510}/[(1 + L)(R_{800} - R_{1510})/(R_{800} + R_{1510} + L)]$ | Herrmann et al., 2010 |
| MCARI _{1510nm} | $MCARI_{1510} = [(R_{700} - R_{1510}) - 0.2 (R_{700} - R_{550})](R_{700}/R_{1510})$ | Herrmann et al., 2010 |
| GnyLi | $GnyLi = (R_{900} \times R_{1050})(R_{955} \times R_{1220})/(R_{900} \times R_{1050}) + (R_{955} \times R_{1220})$ | Gny et al., 2014 |
| Norm. Diff. N. Index | $NDNI = \log(1/R_{1510}) - \log(1/R_{1680})/(\log(1/R_{1510}) + \log(1/R_{1680}))$ | Serrano et al., 2002 |
| N _{1645,1715} | $N_{1645,1715} = (R_{1645} - R_{1715})/(R_{1645} + R_{1715})$ | Pimstein et al., 2011 |
| N _{870,1450} | $N_{870,1450} = (R_{870} - R_{1450})/(R_{870} + R_{1450})$ | Pimstein et al., 2011 |
| N _{850,1510} | $N_{850,1510} = (R_{850} - R_{1510})/(R_{850} + R_{1510})$ | This study |

Table 3
Ranges of the main variables used in the PROSPECT-SAILH radiative transfer model inversions.

| Model | Symbol | Quantity | Ranges | Step | Unit |
|-----------------|------------------------|--|--------------|--------|---------------------|
| PROSPECT | N-struct | Leaf structure parameter | 1.25–1.85 | 0.1 | ... |
| | C _{ab} | Chlorophyll a + b content | 10–70 | 0.5 | μg cm ⁻² |
| | C _w | Equivalent water thickness | 0.001–0.05 | 0.0005 | g cm ⁻² |
| | C _m | Dry matter content | 0.001–0.05 | 0.0005 | g cm ⁻² |
| | C _s | Brown pigment content | 0 | ... | ... |
| SAILH | Sl | Hot-spot parameter | 0.001 | ... | ... |
| | LAI | Leaf area index | 2–5 | 0.1 | ... |
| | LADF | Leaf inclination distribution function | 1,2,3 and 4* | ... | ... |
| | TV | Solar zenith angle | 45°,60°,85° | 5 | deg |
| | Phi | Viewing zenith angle | 0° | ... | deg |
| PSR | Relative azimuth angle | 0° | ... | deg | |

*Canopy types proposed to define LADF: planophile (1), erectophile (2), plagiphile (3) and spherical (4).

variables C_{ab}, C_w and C_m according to Table 3. LADF was firstly retrieved by model inversion, given its key role on canopy structure; 2) the mesophyll structure parameter (N-struct) and leaf area index (LAI) were simultaneously determined over the range 960–1300 nm once the LADF had been fixed to the value retrieved in the first step, and with variable C_{ab}, C_w and C_m according to Table 3; 3) C_{ab} was determined over the range 455–690 nm, with C_w and C_m according to Table 3, fixing LADF, LAI and N determined in previous steps; 4) C_w and C_m were concurrently retrieved over 900–1700 nm, where water and dry matter have the largest absorption effects (Baret and Fourty, 1997; Feret et al., 2008; Fourty et al., 1996; Jacquemoud et al., 2009, 1996).

The accuracy of the estimated parameters (LADF, N-struct, LAI, C_{ab}, C_w and C_m) via model inversion was evaluated by the RMSE calculated between the simulated and measured canopy spectral reflectance. For each standard model inversion, a total of 500000 inversions were carried in forward mode, whereas a total of 200000 inversions were used for the inversion method by steps. Finally, the coefficient of

determination (r²) was calculated to investigate the relationship between the retrieved biophysical parameters (C_{ab}, C_w and C_m) obtained by PROSPECT-SAILH model inversion and the ground-truth physiological measurements.

2.6. Statistical analysis

Stepwise multiple regression analysis using forward mode and leave-one-out-cross-validation (LOOCV) techniques were employed to select the best model to quantify N concentration using i) biophysical parameters derived from the different model inversion methods described above, ii) using narrow-band spectral indices calculated from the VNIR and NIR-100 hyperspectral imagery; and iii) evaluating the performance of the models with the addition of chlorophyll fluorescence quantified from the hyperspectral imagery. Therefore, statistical tests were employed to assess the robustness of each regression model built for nitrogen quantification with and without including solar-induced fluorescence emission retrieved from hyperspectral imagery. A residual analysis model was used to assess the independence of the residual, and the Shapiro-Wilk test for homoscedasticity to verify the normal distribution. The F-test was used to test the significance of the linear regression model, and Student's t-test for the significance of individual regression coefficients. Independent data sets were used for the statistical analysis, using a training data set to build a multiple regression, and an independent second data set to assess the performance of each model under rainfed and irrigated conditions. The training data set comprised the plots located in EC, CA and SA-1, in which the main physiological measurements were made. The test data set was built by SA-1 and SA-2 plots and separated under rainfed and irrigated conditions.

The mean absolute error (MAE), root mean square error (RMSE), mean percentage error (MPE), mean absolute percentage error (MAPE) and coefficient of determination (r²) between the measured leaf nitrogen content and predicted values were used as skill scores to validate the performance of each model. The statistical analysis was conducted in R software (R Core Team, 2015).

Table 4

Average N concentration (%), chlorophyll content derived from SPAD (C_{ab} ; $\mu\text{g cm}^{-2}$), net assimilation (A ; $\mu\text{mol m}^{-2} \text{s}^{-1}$), stomatal conductance (G_s ; $\text{mmol m}^{-2} \text{s}^{-1}$), leaf-water potential (ψ_L ; MPa) and chlorophyll fluorescence (SIF in $\text{Watt sr}^{-1} \text{m}^{-2} \text{nm}^{-2}$), under rainfed and irrigated conditions at EC, CA, SA-1 and SA-2. The standard deviation is also shown.

| | N concentration | C_{ab} (SPAD) | A | G_s | ψ_L | SIF |
|-----------|-----------------|-----------------|------------|---------------|------------|-------------|
| Rainfed | | | | | | |
| EC | 2.50 ± 0.46 | 23.4 ± 3.7 | 7.7 ± 2.1 | 61.27 ± 2 | -2.3 ± 0.2 | 3.74 ± 0.62 |
| CA | 3.28 ± 0.34 | 28.0 ± 3.6 | 11.3 ± 2.1 | 71 ± 24.8 | -2.5 ± 0.4 | 4.22 ± 0.25 |
| SA-1 | 4.17 ± 0.19 | 35.0 ± 3.2 | 17.0 ± 3.3 | 185.8 ± 56.1 | -2.4 ± 0.2 | 4.88 ± 0.57 |
| SA-2 | 2.63 ± 0.32 | 26.0 ± 2.4 | 10.0 ± 2.5 | 121.8 ± 40.5 | -2.7 ± 0.2 | 4.01 ± 0.40 |
| Irrigated | | | | | | |
| CA | 3.37 ± 0.04 | 28.5 ± 2.3 | 14.7 ± 4.1 | 270.6 ± 65.4 | -2.1 ± 0.1 | 4.38 ± 0.17 |
| SA-1 | 4.29 ± 0.28 | 35.8 ± 4.1 | 24.4 ± 2.4 | 354.6 ± 109.4 | -1.7 ± 0.2 | 5.71 ± 0.29 |
| SA-2 | 2.95 ± 0.31 | 29.3 ± 3.9 | 18.3 ± 2.4 | 283.2 ± 65.2 | -2.2 ± 0.1 | 5.14 ± 0.28 |

3. Results

3.1. Field measurements

Mean values of the field physiological measurements and chlorophyll fluorescence retrieved from the airborne imagery for each field site under rainfed and irrigated conditions are shown in Table 4. The results revealed wide variations in the crop physiological status on all sites. As expected, the irrigated plots displayed overall better water and nutritional status than the rainfed plots. There were differences among the rainfed plots; average values of mean N concentration, assimilation rate (A), G_s , and SIF were lower in EC and SA-2 compared to CA and SA-1 (Table 4). The irrigated plots at SA-1, which were at an earlier stage of growth, and at SA-2, displayed an overall better water and nutritional status. These data confirmed the water and nutrient stress conditions in rainfed plots and a large variability among plots.

3.2. Nitrogen concentration and narrow-band hyperspectral indices

The solar induced fluorescence emission and narrow-band reflectance indices calculated from hyperspectral imagery were assessed against field measurements of nitrogen content, chlorophyll content measured with SPAD, and net assimilation (Table 5). The results showed that the NIR/SWIR-based NIs were marginally better predictors of nitrogen content than the VNIR indices, with the MCARI_{1510} and the NDNI (Fig. 4a) indices yielding the best correlation with nitrogen content ($r^2 = 0.69$; $p\text{-value} \leq 0.005$) as compared to MCARI ($r^2 = 0.63$) and PSSRb ($r^2 = 0.63$). The NIs that were modified to replace the 670 nm band by the 1510 nm band due to its relationship with nitrogen absorption (TCARI_{1510} , MCARI_{1510} , $\text{TCARI}/\text{OSAVI}_{1510}$) performed higher at quantifying canopy nitrogen content than their corresponding VNIR-based indices. The $\text{N}_{1645/1715}$ using exclusively reflectance in the SWIR domain showed significant relationship with N content ($r^2 = 0.64$, $p\text{-value} < 0.005$) but still marginally inferior to MCARI_{1510} and NDNI. Table 5 also shows that the indices most sensitive to canopy structure yielded significant relationships with nitrogen content ($r^2 = 0.57$; $p\text{-value} < 0.005$; NDVI). However, the structural indices exhibited saturation over dense canopy, as shown in Fig. 4b for NDVI which tends to saturate due to the higher canopy density at high nitrogen levels. Among the chlorophyll indices used in this study, PSSRb (Fig. 4c) obtained the best results for chlorophyll content estimation ($r^2 = 0.57$, $p\text{-value} \leq 0.0005$), yielding better results than NIs. The airborne-quantified chlorophyll fluorescence was also sensitive to nitrogen content ($r^2 = 0.51$; $p\text{-value} \leq 0.005$) and to the assimilation rate ($r^2 = 0.74$; $p\text{-value} \leq 0.005$; Fig. 4d), confirming other studies that demonstrated the link between airborne-retrieved chlorophyll fluorescence and the photosynthetic activity.

Table 5

Coefficient of determination (r^2) and level of significance for the narrow-band hyperspectral indices and the solar induced chlorophyll fluorescence (SIF; $\text{Watt m}^{-2} \text{sr}^{-1} \text{nm}^{-1}$) quantified from hyperspectral imagery against N concentration, chlorophyll content derived from SPAD values (C_{ab} -SPAD; $\mu\text{g cm}^{-2}$) and net assimilation (A ; $\mu\text{mol m}^{-2} \text{s}^{-1}$).

| Indices | N concentration | | C_{ab} -SPAD | | Net assimilation (A) | |
|------------------------------------|-----------------|-----------|----------------|-----------|----------------------|----------|
| | r^2 | p-value | r^2 | p-value | r^2 | p-value |
| Structural Indices | | | | | | |
| NDVI | 0.57 | < 2.2e-16 | 0.53 | < 2.2e-16 | 0.55 | 1.61e-8 |
| OSAVI | 0.56 | < 2.2e-16 | 0.49 | < 2.2e-16 | 0.53 | 3.23e-8 |
| RDVI | 0.56 | < 2.2e-16 | 0.48 | < 2.2e-16 | 0.53 | 3.92e-8 |
| MCARI/MTVI2 | 0.40 | 2.14e-13 | 0.25 | 2.14e-13 | 0.46 | 5.61e-7 |
| Chlorophyll a + b indices | | | | | | |
| TCARI | 0.54 | < 2.2e-16 | 0.51 | < 2.2e-16 | 0.60 | 1.02e-9 |
| TCARI/OSAVI | 0.45 | 1.78e-15 | 0.30 | 8.64e-10 | 0.51 | 8.59e-8 |
| MCARI | 0.63 | < 2.2e-16 | 0.55 | < 2.2e-16 | 0.57 | 4.78e-9 |
| PSSRb | 0.63 | < 2.2e-16 | 0.57 | < 2.2e-16 | 0.66 | 3.72e-11 |
| GMI | 0.36 | 8.32e-12 | 0.39 | 2.90e-13 | 0.47 | 3.62e-7 |
| GM2 | 0.52 | < 2.2e-16 | 0.47 | 2.22e-16 | 0.26 | 4.79e-4 |
| VOG1 | 0.35 | 4.65e-10 | 0.32 | 1.75e-10 | 0.66 | 3.72e-11 |
| CI | 0.31 | 1.31e-11 | 0.35 | 1.48e-11 | 0.47 | 3.62e-7 |
| Nitrogen Indices | | | | | | |
| DCNI | 0.56 | < 2.2e-16 | 0.50 | < 2.2e-16 | 0.59 | 1.77e-9 |
| TCARI_{1510} | 0.56 | < 2.2e-16 | 0.44 | 1.78e-15 | 0.59 | 1.57e-9 |
| $\text{TCARI}/\text{OSAVI}_{1510}$ | 0.52 | 2.35e-18 | 0.41 | 7.47e-14 | 0.63 | 2.26e-10 |
| MCARI_{1510} | 0.69 | < 2.2e-16 | 0.56 | < 2.2e-16 | 0.43 | 1.86e-6 |
| GnyLi | 0.31 | 3.41e-10 | 0.31 | 2.36e-10 | 0.51 | 7.98e-8 |
| NDNI | 0.69 | < 2.2e-16 | 0.49 | < 2.2e-16 | 0.61 | 5.75e-10 |
| N_{1645} | 0.64 | < 2.2e-16 | 0.52 | < 2.2e-16 | 0.59 | 1.57e-9 |
| $\text{N}_{850-1450}$ | 0.64 | < 2.2e-16 | 0.55 | < 2.2e-16 | 0.63 | 2.26e-10 |
| $\text{NI}_{850/1510}$ | 0.65 | < 2.2e-16 | 0.53 | < 2.2e-16 | 0.61 | 5.75e-10 |
| Fluorescence | | | | | | |
| SIF | 0.51 | < 2.2e-16 | 0.35 | 1.37e-11 | 0.74 | 1.19e-11 |

3.3. Nitrogen content and plant traits estimated by model inversion

The coefficient of determination (r^2) calculated between chlorophyll content (C_{ab}), water content (C_w) and dry matter content (C_m) estimated by PROSPECT-SAILH model inversion and leaf-level physiological measurements (nitrogen content, net assimilation rate and chlorophyll content) are shown in Table 6. These results correspond with the method proposed in Wang et al. (2015) that used biophysical parameters retrieved by model inversion to evaluate the retrieval of leaf N concentration. In the present study, C_{ab} estimated by model inversion by steps correlated with N concentration ($r^2 = 0.71$; $p\text{-value} \leq 0.0005$; Fig. 5a), field-measured leaf C_{ab} ($r^2 = 0.81$; $p\text{-value} \leq 0.0005$; Fig. 5b) and with the assimilation rate ($r^2 = 0.59$; $p\text{-value} \leq 0.0005$; Fig. 5c). Using this model-inversion approach by steps, the relationship between estimated and measured C_{ab} content adjusted well with the 1:1 line for the entire dataset (Fig. 5b), yielding a RMSE = $2.04 \mu\text{g cm}^{-2}$ and MAPE = 5.44%. The two standard model-inversion methods (INV-1

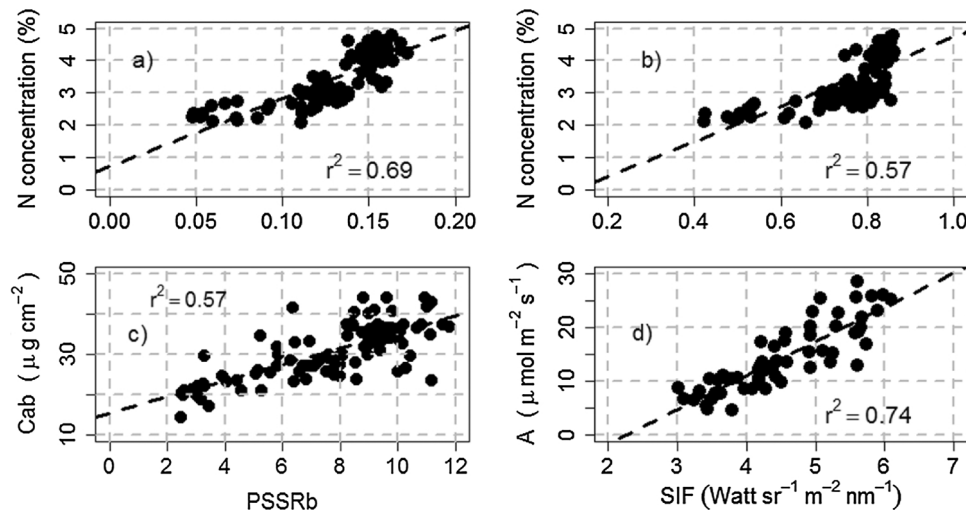


Fig. 4. Relationships between N concentration (in%) vs. NDNI (a) and NDVI (b), C_{ab} vs. PSSRb (c) and A vs. airborne-quantified SIF (d). For all relationships the significance level was $p \leq 0.0005$.

Table 6

Coefficient of determination (r^2) between estimated leaf C_{ab} , C_m and C_w parameters by PROSPECT-SAILH model inversion by steps and by standard inversion methods (INV-1 and INV-2) vs. N concentration, leaf-measured C_{ab} with SPAD, and net assimilation (A).

| | N concentration | C_{ab} (SPAD) | Net Assimilation (A) |
|--|-----------------|-----------------|----------------------|
| Chlorophyll content a + b (C_{ab}) | | | |
| By step | 0.71** | 0.81** | 0.59** |
| INV-1 | 0.012 | 0.008 | 0.001 |
| INV-2 | 0.004 | 0.002 | 0 |
| Equivalent water thickness (C_w) | | | |
| By step | 0.66** | 0.56** | 0.53** |
| INV-1 | 0.017 | 0.008 | 0.008 |
| INV-2 | 0.27** | 0.25** | 0.19* |
| Dry-matter content (C_m) | | | |
| By step | 0.23** | 0.1 | 0.18** |
| INV-1 | 0.49** | 0.32** | 0.30** |
| INV-2 | 0.38* | 0.24** | 0.23** |

** p-value < 0.0005; * p-value < 0.02.

and INV-2) displayed quite different behavior; C_{ab} was correctly estimated for plots with N concentration and C_{ab} values that were higher than 3.5% and $30 \mu\text{g cm}^{-2}$ respectively, while the retrievals failed for the plots with nitrogen and C_{ab} values below these (see outliers in Fig. 5b). The two standard model inversion approaches thus yielded weaker results in their estimates of nitrogen content (RMSE $\geq 6.33 \mu\text{g cm}^{-2}$ and MAPE $\geq 17.68\%$) than the model inversion by steps.

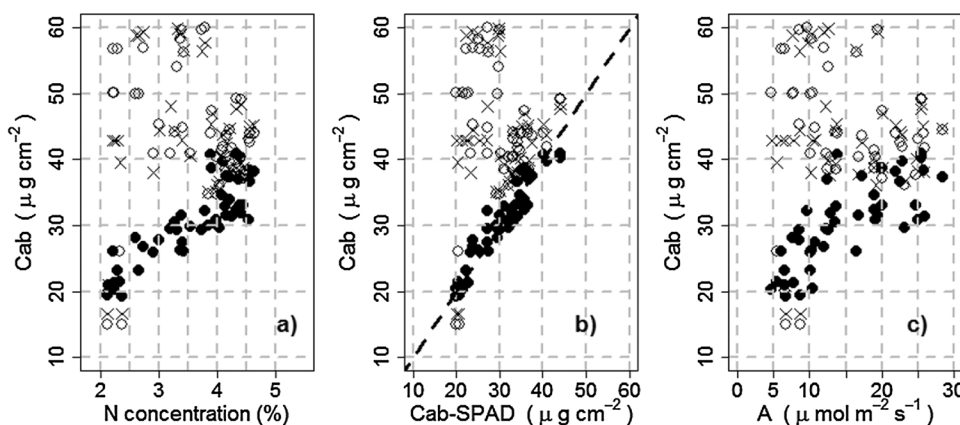


Fig. 5. Chlorophyll content (C_{ab} , $\mu\text{g cm}^{-2}$) estimated by model inversions vs. N concentration (in%) (a), chlorophyll content derived from SPAD (C_{ab} -SPAD; $\mu\text{g cm}^{-2}$) (b), and leaf assimilation rate (A, $\mu\text{mol m}^{-2} \text{s}^{-1}$) (c). Black points correspond to inversion by steps, black crosses using the INV-1 method and open black circles using the INV-2 model inversion method. The dashed line is the 1:1 line.

Leaf equivalent water thickness retrieval by model inversion was significantly related to N concentration ($r^2 = 0.66$; p -value ≤ 0.0005), while dry matter content showed significant (yet lower coefficients of determination than for C_w) yielding $r^2 = 0.23$ (step inversion method) and $r^2 = 0.49$ (INV-1 method) (in both cases p -value ≤ 0.0005). In this case, the coefficient of determination was significantly affected by outliers, inducing an artificial increase in the correlation coefficients for INV-1 as compared to the step inversion method. In summary, the three leaf biochemical parameters C_{ab} , C_w and C_m estimated by radiative transfer model inversion from the hyperspectral imagery were significantly related to leaf N concentration (p -value ≤ 0.0005 in all three cases), but C_{ab} and C_w yielded higher relationship with N than C_m .

3.4. Leaf N estimation from the airborne hyperspectral imagery accounting for chlorophyll fluorescence

The stepwise multiple regression and LOOCV methods built to estimate N concentration using the leaf biochemical constituents C_{ab} , C_w and C_m obtained by model inversion, were assessed accounting for the contribution of adding chlorophyll fluorescence. The statistical models built using all input parameters, with and without including SIF as predictor of nitrogen are shown in Table 7. The homoscedasticity and the normal distribution requirements were satisfied and passed the statistical test (F-Test). According to the t -test, the regression coefficients for C_{ab} and SIF were significant at the 5% significance level. In contrast, C_m and C_w parameters were non-significant in some of the regression models (see Table 7).

Table 7
Statistical tests for the validity of the regression models used to estimate N concentration.

| | F-test | | Shapiro-Wilk | p-value (t-test) | | | |
|--|---------|------|--------------|------------------|-----------------|----------------|----------------|
| | p-value | W | | p-value | C _{ab} | C _w | C _m |
| Without Fluorescence | | | | | | | |
| N = f(C _{ab}) | 2.4E-13 | 0.98 | 0.55 | 2.4e-13 | | | |
| N = f(C _{ab} , C _w) | 2.9E-16 | 0.98 | 0.64 | 6.2e-6 | 0.0003 | | |
| N = f(C _{ab} , C _m) | 7.5E-17 | 0.98 | 0.46 | 7.6e-14 | | 8.2e-5 | |
| N = f(C _{ab} , C _w , C _m) | 6.4E-17 | 0.98 | ≥ 0.05 | 8.7e-6 | 0.5911 | 0.0906 | |
| With Fluorescence | | | | | | | |
| N = f(C _{ab} , SIF) | 8.2E-27 | 0.97 | 0.35 | 7.8e-10 | 1.1e-14 | | |
| N = f(C _{ab} , C _w , SIF) | 1.4E-28 | 0.96 | 0.17 | 1.0e-6 | 0.0059 | | 2.7e-13 |
| N = f(C _{ab} , C _m , SIF) | 1.1E-27 | 0.97 | 0.23 | 1.9e-10 | | 0.0519 | 7.2e-12 |
| N = f(C _{ab} , C _w , C _m , SIF) | 1.2E-28 | 0.97 | 0.2 | 0.0013 | 0.0429 | 0.5395 | 1.8e-12 |

Table 8
Performance of the regression models built to estimate N concentration using r², RMSE, ME, MAE, MAPE and standardized coefficients as performance indicators.

| Regression Models | r ² | RMSE | MAE | MAPE | Standard. coefficients (β ₀) | | | |
|--|----------------|------|------|-------|--|----------------|----------------|------|
| | | | | | C _{ab} | C _w | C _m | SIF |
| Without Fluorescence | | | | | | | | |
| N = f(C _{ab}) | 0.68 | 0.47 | 0.39 | 12.0% | 0.84 | ... | ... | ... |
| N = f(C _{ab} , C _w) | 0.74 | 0.41 | 0.34 | 9.9% | 0.54 | 0.41 | ... | ... |
| N = f(C _{ab} , C _m) | 0.77 | 0.40 | 0.33 | 9.7% | 0.77 | ... | -0.31 | ... |
| N = f(C _{ab} , C _w , C _m) | 0.75 | 0.41 | 0.34 | 10.0% | 0.70 | 0.11 | -0.24 | ... |
| With Fluorescence | | | | | | | | |
| N = f(C _{ab} , SIF) | 0.92 | 0.23 | 0.19 | 5.9% | 0.43 | ... | ... | 0.63 |
| N = f(C _{ab} , C _w , SIF) | 0.92 | 0.22 | 0.18 | 5.6% | 0.34 | 0.17 | ... | 0.57 |
| N = f(C _{ab} , C _m , SIF) | 0.92 | 0.23 | 0.19 | 5.9% | 0.44 | ... | -0.10 | 0.57 |
| N = f(C _{ab} , C _w , C _m , SIF) | 0.93 | 0.20 | 0.18 | 5.5% | 0.30 | 0.23 | 0.05 | 0.58 |

The ability of each model to predict N concentration was assessed using the LOOCV scores described earlier, showing the results in Table 8. Based on these statistical scores, the multiple linear regression models using SIF as predictive variable considerably improved the accuracy of N estimation ($r_{LOOCV}^2 \geq 0.92$; $MAE_{LOOCV} \leq 0.19$ and $RMSE_{LOOCV} \leq 0.23$). As a comparison, regression models without including fluorescence (SIF) reached significantly lower predictive power ($r_{LOOCV}^2 \leq 0.77$; $MAE_{LOOCV} \geq 0.33$ and $RMSE_{LOOCV} \geq 0.40$). The contribution of each variable is shown by standardized coefficients (β_0 ; Table 8). These results show that in models that include SIF as predictor, its contribution to the retrieval of N was higher than the rest of the predictors, being almost double than the contribution of C_{ab}. In the models that did not use SIF as predictor, the estimated C_{ab} by model inversion contributed the highest to N estimation.

According to r², RMSE, MAE and MAPE, the most accurate estimation was achieved by the regression model when the predictors were C_{ab}, C_w, C_m and SIF, yielding $r_{LOOCV}^2 = 0.93$, $RMSE_{LOOCV} = 0.20$, $MAE_{LOOCV} = 0.18$ and the lowest MAPE (Table 8). Nevertheless, the rest of models with less number of parameters (therefore simpler) obtained accuracies only marginally lower (e.g. $r^2 = 0.93$ & $RMSE = 0.20$ for the most complex model using C_{ab}, C_w, C_m and SIF as compared to $r^2 = 0.92$ & $RMSE = 0.23$ for the model using C_{ab} and SIF). Fig. 6 shows the scatter plots between the measured and predicted N concentration using the model without (top plots) and with SIF as predictor (bottom plots). The models using SIF showed lower RMSE and better performance than the rest of the models that did not employ fluorescence as predictor.

Based on these results, the proposed models combining leaf biochemical constituents with and without SIF were evaluated as predictors for N concentration separately for rainfed and irrigated conditions. All models showed greater accuracies in predicting N concentration under rainfed (stress) conditions than under irrigated (non-water stress) conditions (e.g. best model performance yielded $r^2 = 0.93$ (rainfed) vs. $r^2 = 0.88$; (irrigated) (Table 9). As Fig. 7 shows, the plots were aligned over the 1:1 line for both cases of rainfed

(Fig. 7a) and irrigated conditions (Fig. 7b). Under rainfed conditions, the models with SIF as predictor yielded significantly higher scores ($r^2 \geq 0.89$, $RMSE \leq 0.26$ and $MAPE \leq 6.8\%$) than models without SIF as predictor ($r^2 \geq 0.78$, $RMSE \leq 0.37$ and $MAPE \leq 9.46\%$).

Under irrigated conditions, the models that used SIF as predictor also showed the best performance. The model built with C_{ab} and SIF displayed better accuracy in predicting nitrogen concentration ($r^2 = 0.65$, $RMSE = 0.42$ and $MAPE \leq 10.6\%$) than the model with C_{ab} only ($r^2 = 0.48$, $RMSE = 0.51$ and $MAPE \leq 12.56\%$), indicating that the contribution of SIF was highly significant under both irrigated and non-irrigated conditions.

These modelling methods enabled the quantification of N concentration from the hyperspectral imagery to show its spatial distribution in the context of precision agriculture and plant phenotyping experiments. Fig. 8 shows the spatial distribution of N concentration using C_{ab}, C_w, C_m and SIF as predictors (Fig. 8a) over plots under rainfed (Fig. 8b) and irrigated conditions (Fig. 8c) at the SA field site during the 2016 campaign. Higher values of nitrogen concentration (blue color) from the rainfed plots indicate a better physiological status, while low N values (red color) indicate stress levels as consequence of the rainfed conditions. In comparison with irrigated conditions, the N map clearly showed the lower values obtained in the rainfed fields, with average values of $3.1 \pm 0.18\%$; under irrigated conditions the average N concentration was higher ($4.2 \pm 0.3\%$). This methodology enables an operational quantification of canopy N concentration at the field level using high resolution hyperspectral remote sensing imagery and radiative-transfer model inversion methods.

4. Discussion

Several studies have focused on the estimation of canopy N concentration using remote sensing techniques. The main problem encountered is that N does not absorb radiation with distinct features to enable its direct quantification with reflectance data. Instead, proxies physiologically related to N which are potentially retrievable from

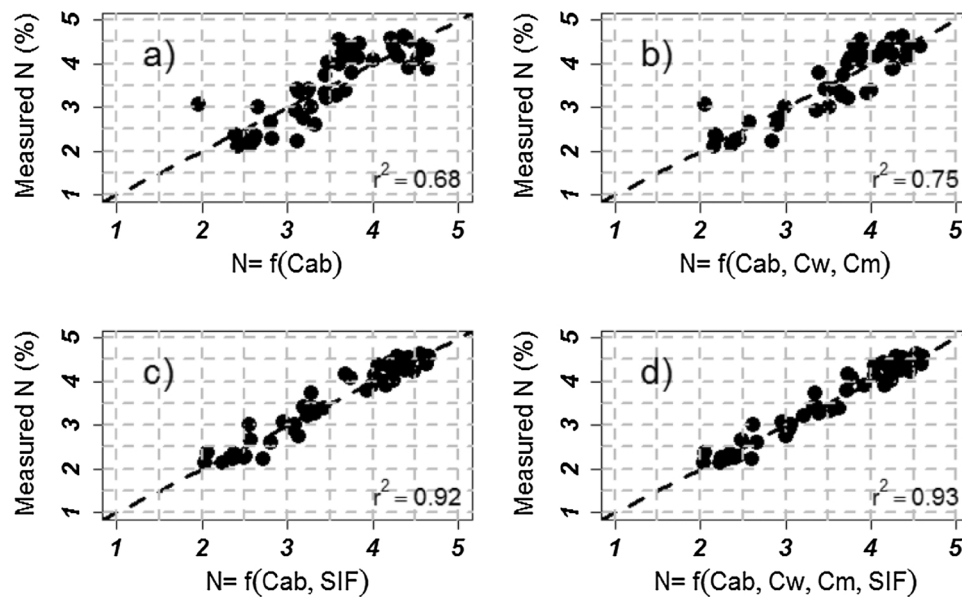


Fig. 6. Measured vs. estimated N concentration using the best regression LOOCV models without fluorescence (a,b) and with fluorescence (c,d) as a function of C_{ab} (a), C_{ab} , C_w and C_m (b), C_{ab} and SIF (c) and C_{ab} , C_w , C_m and SIF (d). The dashed line is the 1:1 line.

Table 9

Statistics for r^2 , RMSE, ME, MAE, MPE and MAPE between measured and predicted N concentration under rainfed and irrigated conditions.

| | r^2 | RMSE | MAE | MPE | MAPE |
|--------------------------------|-------|------|------|--------|--------|
| Rainfed conditions | | | | | |
| Without Fluorescence | | | | | |
| $N = f(C_{ab})$ | 0.78 | 0.37 | 0.29 | -1.44% | 9.46% |
| $N = f(C_{ab}, C_m)$ | 0.81 | 0.34 | 0.27 | -1.12% | 8.50% |
| $N = f(C_{ab}, C_w)$ | 0.86 | 0.36 | 0.23 | -0.92% | 7.54% |
| $N = f(C_{ab}, C_w, C_m)$ | 0.86 | 0.29 | 0.23 | -0.84% | 7.24% |
| With Fluorescence | | | | | |
| $N = f(C_{ab}, SIF)$ | 0.89 | 0.26 | 0.21 | -0.65% | 6.89% |
| $N = f(C_{ab}, C_m, SIF)$ | 0.89 | 0.26 | 0.22 | -0.64% | 6.86% |
| $N = f(C_{ab}, C_w, SIF)$ | 0.92 | 0.23 | 0.18 | -0.45% | 5.68% |
| $N = f(C_{ab}, C_w, C_m, SIF)$ | 0.93 | 0.22 | 0.18 | -0.45% | 5.65% |
| Irrigated conditions | | | | | |
| Without Fluorescence | | | | | |
| $N = f(C_{ab})$ | 0.48 | 0.51 | 0.44 | -2.03% | 12.56% |
| $N = f(C_{ab}, C_m)$ | 0.59 | 0.45 | 0.37 | -1.65% | 10.50% |
| $N = f(C_{ab}, C_w)$ | 0.76 | 0.35 | 0.29 | -0.89% | 8.05% |
| $N = f(C_{ab}, C_w, C_m)$ | 0.77 | 0.34 | 0.28 | -0.85% | 7.68% |
| With Fluorescence | | | | | |
| $N = f(C_{ab}, SIF)$ | 0.65 | 0.42 | 0.36 | -1.41% | 10.6% |
| $N = f(C_{ab}, C_m, SIF)$ | 0.77 | 0.34 | 0.27 | -0.93% | 7.89% |
| $N = f(C_{ab}, C_w, SIF)$ | 0.84 | 0.28 | 0.34 | -0.58% | 6.77% |
| $N = f(C_{ab}, C_w, C_m, SIF)$ | 0.88 | 0.25 | 0.20 | -0.47% | 5.63% |

remote sensing spectra are proposed as the only feasible way of detecting nitrogen levels under nutrient-deficiency conditions. An example is the widely used SPAD meter, a hand held instrument that measures chlorophyll content and generally accepted to track N concentration at the leaf level (Ravier et al., 2017). Most of the studies that assess the retrieval of N through non-destructive methods have been traditionally based on empirical models with spectral indices (i.e. spectral proxies) calculated from the visible (VIS) and near-infrared (NIR) regions (Clevers and Kooistra, 2012; Li et al., 2014), while only a few studies focused on radiative transfer model inversions and the relationships between retrieved parameters (i.e. biophysical parameters and biochemical constituents as proxies) and nitrogen (Thorp et al., 2012; Wang et al., 2015). The present study evaluated these standard hyperspectral remote sensing techniques for the estimation of N concentration using narrow-band indices combining the VNIR and the SWIR region, but focusing on the potential contribution of a new

indicator such as the radiance-based fluorescence SIF for improving the performance of N estimation. According to the results obtained by the regression models built with C_{ab} , C_w , C_m and SIF from the stepwise multiple regression and LOOCV methods, the solar induced chlorophyll fluorescence quantified from the hyperspectral imagery significantly increased the performance for the estimation of N. This result confirms the findings of other studies that suggested a close link between fluorescence emission and nitrogen (Corp et al., 2003; Schächtl et al., 2005; Cendrero-Mateo et al., 2016). The contribution of SIF to predict N concentration was higher than that of C_{ab} and leaf biochemical parameters such as dry matter and equivalent water thickness. In fact, models containing fluorescence emission among their predictors produced the most reliable nitrogen estimation when compared to models without SIF. The results indicated that SIF retrieval by the FLD method from high resolution hyperspectral imagery demonstrated its value for monitoring N concentration under both rainfed and irrigated conditions in the context of precision agriculture and plant phenotyping studies. The solar induced chlorophyll fluorescence provides a potential new tool to estimate canopy N concentration, due to their close link with photosynthetic parameters such as the maximum rate of carboxylation and with plant functioning. These results agree with recent studies that showed the ability of such methods to evaluate crop physiological status under conditions of water stress, compared to hyperspectral narrow-band indices (Herrmann et al., 2010; Ranjan et al., 2012; Gonzalez-Dugo et al., 2015; Zarco-Tejada et al., 2016). This study also demonstrates that the biophysical parameters retrieved from a radiative transfer model at canopy scale are needed for better N concentration estimation due to the more robust quantification of the parameters as compared to single narrow-band hyperspectral indices. This agrees with Wang et al. (2015) who demonstrated that the combination of biophysical parameters (leaf chlorophyll, dry matter and water content) retrieved via PROSPECT model inversion provided a reliable tool to estimate N at leaf scale. They found a higher correlation between leaf nitrogen content and dry matter and water content than with chlorophyll. Our results indicate that, in the absence of chlorophyll fluorescence as predictor, chlorophyll a + b was the parameter most related with nitrogen. This result is in agreement with other studies that indicate that the chlorophyll is the most widely used proxy for N estimation (Herrmann et al., 2010; Homolová et al., 2013). In this regard, this study displayed that C_w and C_m contributions for predicting nitrogen concentration were lower than C_{ab} and SIF in both rainfed and

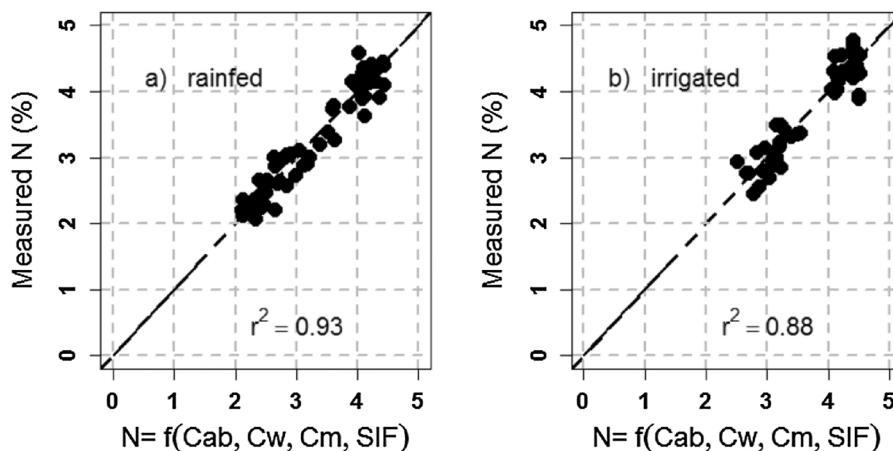


Fig. 7. Measured vs. estimated N concentration for rainfed (a) and irrigated conditions (b) using the model built with C_{ab} , C_m and C_w biochemical constituents (estimated by model inversion) including fluorescence. The solid line is the 1:1 line.

irrigated conditions. However, it was observed that under irrigated conditions the models showed lower accuracy at predicting N concentration, especially when C_{ab} was the only predictor. Under the conditions of this experiment, the lower performance obtained for irrigated vs. rainfed conditions was likely due to the smaller range of variability found for the predictors in the irrigated than in the rainfed plots. The results of this study showed that the contribution of SIF (which can be also derived from VNIR cameras) is superior than the contribution of the NIR-SWIR camera used here to estimate dry matter and equivalent water thickness. Considering the cost, complexity of operation, and the lower resolution generally obtained by SWIR cameras, the interest of retrieving SIF and chlorophyll content from a single VNIR camera outperforms the SWIR under the conditions and objectives of the present study.

This work also demonstrates that the model inversion by steps yields more reliable retrievals than traditional inversions, which used the entire VNIR up to 1700 nm region to retrieve all parameters simultaneously. This result shows that model inversions conducted by steps reduced the ill-posed inverse problems (Combal et al., 2003; Wang et al., 2007; Yebra and Chuvieco, 2009; Li and Wang, 2011) and

improves the parameter retrievals. Our results also confirm findings by Li and Wang (2011) regarding this issue.

Another important result obtained in this study shows that the regression models built with parameters obtained by model-inversion yielded superior results than simple linear models based on spectral indices (Herrmann et al., 2010; Pimstein et al., 2011; Bao et al., 2013; Mahajan et al., 2014; Gnyp et al., 2014). This conclusion was true even when using narrow-band indices centered at 1510 and 850 nm, which are highly correlated with N concentration. Regarding hyperspectral indices, our results confirmed findings reported by Herrmann et al. (2010) that the use of the SWIR domain significantly improved the estimation of nitrogen concentration when compared to the visible and near-infrared region of the spectrum. In our case, the use of the SWIR spectral range to determine NIs provided better quantification of N concentration than when only the VNIR region was used, in particular when using indices from bands centered at 1510 nm (Herrmann et al., 2010; Serrano et al., 2002). Among all indices, the NIs that combined 1510 nm and VNIR bands yielded the highest agreement with N concentration (e.g. $r^2 = 0.69$ for $MCARI_{1510}$ and $r^2 = 0.65$ for $NI_{1850/1510}$). However, these simple relationships obtained between N concentration

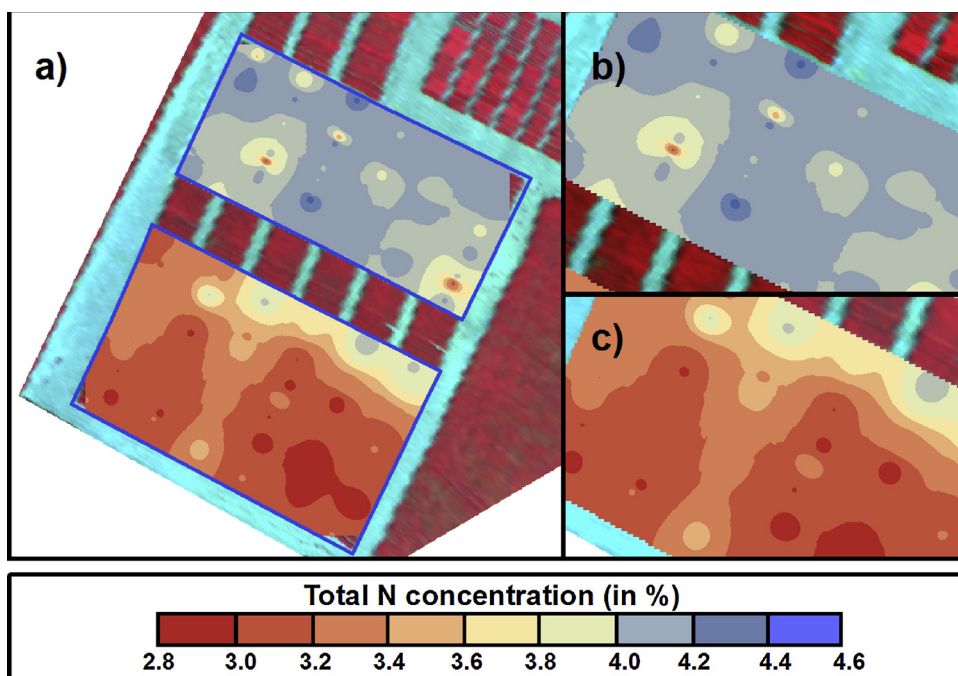


Fig. 8. Map showing the spatial distribution of N concentration estimated using the model built with chlorophyll a + b (C_{ab}), water content (C_w), dry matter content (C_m) and solar induced chlorophyll fluorescence (SIF) estimated from hyperspectral imagery (a) and used as predictors under irrigated (b) and rainfed (c) conditions at SA field site during the 2016 airborne campaign.

and chlorophyll indices are affected by structure and the underlying soil. By contrast, the structural indices (e.g. NDVI) tend to saturate their values under dense canopies and with high nitrogen levels (Fig. 4b). Nevertheless, none of the hyperspectral index combinations outperformed the results obtained by model inversion when adding fluorescence (i.e. $C_{ab} + C_m + C_w + SIF$), which was by far the best model for N estimation.

An additional important topic is that the methodology used here for the airborne retrieval of chlorophyll fluorescence from radiance imagery is based on the work presented in previous studies (e.g.: Damm et al., 2015; Zarco-Tejada et al., 2016), confirming that the use of hyperspectral imagery acquired at broader spectral bands (i.e. with FWHM 2–7 nm) retains sufficient chlorophyll fluorescence signal to yield the most significant relationships against field-measured assimilation rates among all other image-derived indicators.

An issue observed in this work is the potential limitations of the plot sizes normally used by plant breeders during their experimental designs. The plot dimension should be compatible with the spatial resolution of the imagery acquired by remote sensing. When the plots are too small, soil and background effects may play a critical role due to the mixing of the different components (i.e. soil and shadows) with the vegetation. This issue is important in the case in of the coarser resolution generally obtained by SWIR cameras. New sensors carried on board drones and low altitude manned aircraft can potentially obtain high- and ultra-high resolutions, which are compatible with the standard phenotyping and plant breeding experiments. Nevertheless, plant breeding experimental design should be compatible with the spatial resolutions of the remote sensing sensors to be flown over the study sites. In this way, a line of at least 1/2 to 1 pixel as edge around the center of the plot is recommended.

5. Conclusions

The present study demonstrates that the airborne-quantified solar induced chlorophyll fluorescence (SIF) is a critical predictor for the estimation of N concentration under semi-arid and arid conditions when combined with chlorophyll a + b content and leaf parameters dry matter (C_m) and equivalent water thickness (C_w) plant traits retrieved by radiative transfer model inversion. When the models were built with airborne-quantified SIF, N estimation performance improved under both rainfed (water-stress) and irrigated conditions. Additionally, the models that combined SIF and chlorophyll a + b content performed better than standard empirical methods based on simple linear relationships with narrow-band hyperspectral indices. In addition, this work demonstrates that SWIR-based indices centered at 1510 nm yield more reliable agreements with N concentration ($r^2 = 0.69$) than traditional chlorophyll indices (TCARI/OSAVI $r^2 = 0.45$) proposed as proxy for N quantification.

Acknowledgments

The authors gratefully acknowledge the financial support of the Spanish Ministry of Science and Education (MEC) for projects AGL2012-40053-C03-01, and AGL2012-35196 and the Junta de Andalucía for projects P12-AGR-2521 and P12-AGR-0482. Dr Ignacio Solis Martel from Agrovetal S.A. is gratefully acknowledged for facilitating access and sampling of their experimental farm. D. Notario, A. Vera, A. Hornero, R. Romero and R. Mérida-García are also thanked for their technical support during the field and airborne campaigns.

References

Bao, Y., Xu, K., Min, J., Xu, J., 2013. Estimating wheat shoot nitrogen content at vegetative stage from in situ hyperspectral measurements. *Crop Sci.* 53, 2063–2071. <http://dx.doi.org/10.2135/cropsci2013.01.0012>.

Baret, F., Fourty, T., 1997. Estimation of leaf water content and specific leaf weight from

reflectance and transmittance measurements. *Agronomie* 17, 455–464. <http://dx.doi.org/10.1051/agro:19970903>.

Baret, F., Jacquemoud, S., Guyot, G., Leprieux, C., 1992. Modeled analysis of the biophysical nature of spectral shifts and comparison with information content of broad bands. *Remote Sens. Environ.* 41, 133–142. [http://dx.doi.org/10.1016/0034-4257\(92\)90073-S](http://dx.doi.org/10.1016/0034-4257(92)90073-S).

Berni, J., Zarco-Tejada, P.J., Suarez, L., Fereres, E., 2009. Thermal and narrowband multispectral remote sensing for vegetation monitoring from an unmanned aerial vehicle. *IEEE Trans. Geosci. Remote Sens.* 47, 722–738. <http://dx.doi.org/10.1109/TGRS.2008.2010457>.

Blackburn, G.A., 1998. Spectral indices for estimating photosynthetic pigment concentrations: a test using senescent tree leaves. *Int. J. Remote Sens.* 19, 657–675. <http://dx.doi.org/10.1080/014311698215919>.

Calderón, R., Navas-Cortés, J.A., Lucena, C., Zarco-Tejada, P.J., 2013. High-resolution airborne hyperspectral and thermal imagery for early detection of Verticillium wilt of olive using fluorescence, temperature and narrow-band spectral indices. *Remote Sens. Environ.* 139, 231–245. <http://dx.doi.org/10.1016/j.rse.2013.07.031>.

Calderón, R., Navas-Cortés, J.A., Zarco-Tejada, P.J., 2015. Early detection and quantification of Verticillium Wilt in olive using hyperspectral and thermal imagery over large areas. *Remote Sens.* 7, 5584–5610. <http://dx.doi.org/10.3390/rs70505584>.

Cendrero-Mateo, M.P., Moran, M.S., Papuga, S.A., Thorp, K.R., Alonso, L., Moreno, J., Ponce-Campos, G., Rascher, U., Wang, G., 2016. Plant chlorophyll fluorescence: active and passive measurements at canopy and leaf scales with different nitrogen treatments. *J. Exp. Bot.* 67, 275–286. <http://dx.doi.org/10.1093/jxb/erv456>.

Chen, P., Haboudane, D., Tremblay, N., Wang, J., Vigneault, P., Li, B., 2010. New spectral indicator assessing the efficiency of crop nitrogen treatment in corn and wheat. *Remote Sens. Environ.* 114, 1987–1997. <http://dx.doi.org/10.1016/j.rse.2010.04.006>.

Clevers, J.G.P.W., Kooistra, L., 2012. Using hyperspectral remote sensing data for retrieving canopy chlorophyll and nitrogen content. *IEEE J. Sel. Top. Appl. Earth Obs. Remote Sens.* 5, 574–583. <http://dx.doi.org/10.1109/JSTARS.2011.2176468>.

Combal, B., Baret, F., Weiss, M., Trubuil, A., Macé, D., Pragnère, A., Myneni, R., Knyazikhin, Y., Wang, L., 2003. Retrieval of canopy biophysical variables from bidirectional reflectance using prior information to solve the ill-posed inverse problem. *Remote Sens. Environ.* 84, 1–15. [http://dx.doi.org/10.1016/S0034-4257\(02\)00035-4](http://dx.doi.org/10.1016/S0034-4257(02)00035-4).

Corp, L.A., McMurtrey, J.E., Middleton, E.M., Mulchi, C.L., Chappelle, E.W., Daughtry, C.S.T., 2003. Fluorescence sensing systems: in vivo detection of biophysical variations in field corn due to nitrogen supply. *Remote Sens. Environ.* 86, 470–479. [http://dx.doi.org/10.1016/S0034-4257\(03\)00125-1](http://dx.doi.org/10.1016/S0034-4257(03)00125-1).

Croft, H., Chen, J.M., Luo, X., Bartlett, P., Chen, B., Staebler, R.M., 2017. Leaf chlorophyll content as a proxy for leaf photosynthetic capacity. *Glob. Change Biol.* 23, 3513–3524. <http://dx.doi.org/10.1111/gcb.13599>.

Damm, A., Erler, A., Hillen, W., Meroni, M., Schaepman, M.E., Verhoef, W., Rascher, U., 2011. Modeling the impact of spectral sensor configurations on the FLD retrieval accuracy of sun-induced chlorophyll fluorescence. *Remote Sens. Environ.* 115, 1882–1892. <http://dx.doi.org/10.1016/j.rse.2011.03.011>.

Damm, A., Guanter, L., Paul-Limoges, E., van der Tol, C., Hueni, A., Buchmann, N., Eugster, W., Ammann, C., Schaepman, M.E., 2015. Far-red sun-induced chlorophyll fluorescence shows ecosystem-specific relationships to gross primary production: an assessment based on observational and modeling approaches. *Remote Sens. Environ.* 166, 91–105. <http://dx.doi.org/10.1016/j.rse.2015.06.004>.

Daughtry, C., 2000. Estimating corn leaf chlorophyll concentration from leaf and canopy reflectance. *Remote Sens. Environ.* 74, 229–239. [http://dx.doi.org/10.1016/S0034-4257\(00\)00113-9](http://dx.doi.org/10.1016/S0034-4257(00)00113-9).

Eitel, J.U.H., Long, D.S., Gessler, P.E., Smith, A.M.S., 2007. Using in-situ measurements to evaluate the new RapidEye™ satellite series for prediction of wheat nitrogen status. *Int. J. Remote Sens.* 28, 4183–4190. <http://dx.doi.org/10.1080/01431160701422213>.

Feret, J.B., François, C., Asner, G.P., Gitelson, A.A., Martin, R.E., Bidol, L.P.R., Ustin, S.L., le Maire, G., Jacquemoud, S., 2008. PROSPECT-4 and 5: advances in the leaf optical properties model separating photosynthetic pigments. *Remote Sens. Environ.* 112, 3030–3043. <http://dx.doi.org/10.1016/j.rse.2008.02.012>.

Ferwerda, J.G., Skidmore, A.K., Mutanga, O., 2005. Nitrogen detection with hyperspectral normalized ratio indices across multiple plant species. *Int. J. Remote Sens.* 26, 4083–4095. <http://dx.doi.org/10.1080/01431160500181044>.

Fourty, T., Baret, F., Jacquemoud, S., Schmuck, G., Verdebout, J., 1996. Leaf optical properties with explicit description of its biochemical composition: direct and inverse problems. *Remote Sens. Environ.* 56, 104–117. [http://dx.doi.org/10.1016/0034-4257\(95\)00234-0](http://dx.doi.org/10.1016/0034-4257(95)00234-0).

Genty, B., Briantais, J.M., Baker, N.R., 1989. The relationship between the quantum yield of photosynthetic electron transport and quenching of chlorophyll fluorescence. *Biochim. Biophys. Acta – Gen. Subj.* 990, 87–92. [http://dx.doi.org/10.1016/S0304-4165\(89\)80016-9](http://dx.doi.org/10.1016/S0304-4165(89)80016-9).

Gitelson, A.A., Merzlyak, M.N., 1997. Remote estimation of chlorophyll content in higher plant leaves. *Int. J. Remote Sens.* 18, 2691–2697. <http://dx.doi.org/10.1080/014311697217558>.

Gnyp, M.L., Bareth, G., Li, F., Lenz-Wiedemann, V.I.S., Koppe, W., Miao, Y., Hennig, S.D., Jia, L., Laudien, R., Chen, X., Zhang, F., 2014. Development and implementation of a multiscale biomass model using hyperspectral vegetation indices for winter wheat in the North China Plain. *Int. J. Appl. Earth Obs. Geoinf.* 33, 232–242. <http://dx.doi.org/10.1016/j.jag.2014.05.006>.

Gonzalez-Dugo, V., Durand, J.-L., Gastal, F., 2010. Water deficit and nitrogen nutrition of crops. A review. *Agron. Sustain. Dev.* 30, 529–544. <http://dx.doi.org/10.1051/agro/2009059>.

Gonzalez-Dugo, V., Hernandez, P., Solis, I., Zarco-Tejada, P.J., 2015. Using high-

- resolution hyperspectral and thermal airborne imagery to assess physiological condition in the context of wheat phenotyping. *Remote Sens.* 7, 13586–13605. <http://dx.doi.org/10.3390/rs71013586>.
- Gueymard, C.A., Myers, D., Emery, K., 2002. Proposed reference irradiance spectra for solar energy systems testing. *Solar Energy* 73, 443–467. [http://dx.doi.org/10.1016/S0038-092X\(03\)00005-7](http://dx.doi.org/10.1016/S0038-092X(03)00005-7).
- Gueymard, C., 1995. SMARTS, a Simple Model of the Atmospheric Radiative Transfer of Sunshine: Algorithms and Performance Assessment. Florida Solar Energy Center, Cocoa, FL Technical report no. FSEC-PF-270–95.
- Haboudane, D., Miller, J.R., Tremblay, N., Zarco-Tejada, P.J., Dextraze, L., 2002. Integrated narrow-band vegetation indices for prediction of crop chlorophyll content for application to precision agriculture. *Remote Sens. Environ.* 81, 416–426. [http://dx.doi.org/10.1016/S0034-4257\(02\)00018-4](http://dx.doi.org/10.1016/S0034-4257(02)00018-4).
- Herrmann, I., Karnieli, A., Bonfil, D.J., Cohen, Y., Alchanatis, V., 2010. SWIR-based spectral indices for assessing nitrogen content in potato fields. *Int. J. Remote Sens.* 31, 5127–5143. <http://dx.doi.org/10.1080/01431160903283892>.
- Homolová, L., Malenovsky, Z., Clevers, J.G.P.W., García-Santos, G., Schaepman, M.E., 2013. Review of optical-based remote sensing for plant trait mapping. *Ecol. Complex* 15, 1–16. <http://dx.doi.org/10.1016/j.ecocom.2013.06.003>.
- Houborg, R., Cescatti, A., Migliavacca, M., Kustas, W.P., 2013. Satellite retrievals of leaf chlorophyll and photosynthetic capacity for improved modeling of GPP. *Agric. For. Meteorol.* 117, 10–23. <http://dx.doi.org/10.1016/j.agrformet.2013.04.006>.
- Jacquemoud, S., Baret, F., 1990. PROSPECT: a model of leaf optical properties spectra. *Remote Sens. Environ.* 34, 75–91. [http://dx.doi.org/10.1016/0034-4257\(90\)90100-Z](http://dx.doi.org/10.1016/0034-4257(90)90100-Z).
- Jacquemoud, S., Ustin, S.L., Verdebout, J., Schmuck, G., Andreoli, G., Hosgood, B., 1996. Estimating leaf biochemistry using the PROSPECT leaf optical properties model. *Remote Sens. Environ.* 56, 194–202. [http://dx.doi.org/10.1016/0034-4257\(95\)00238-3](http://dx.doi.org/10.1016/0034-4257(95)00238-3).
- Jacquemoud, S., Verhoef, W., Baret, F., Bacour, C., Zarco-Tejada, P.J., Asner, G.P., François, C., Ustin, S.L., 2009. PROSPECT + SAIL models: a review of use for vegetation characterization. *Remote Sens. Environ.* 113, S56–S66. <http://dx.doi.org/10.1016/j.rse.2008.01.026>.
- Jin, X., Yang, G., Tan, C., Zhao, C., 2015. Effects of nitrogen stress on the photosynthetic CO₂ assimilation, chlorophyll fluorescence, and sugar-nitrogen ratio in corn. *Sci. Rep.* 5, 9311. <http://dx.doi.org/10.1038/srep09311>.
- Khamis, S., Lamaze, T., Lemoine, Y., Foyer, C., 1990. Adaptation of the photosynthetic apparatus in maize leaves as a result of nitrogen limitation: relationships between electron transport and carbon assimilation. *Plant Physiol.* 94, 1436–1443. <http://dx.doi.org/10.1104/pp.94.3.1436>.
- Kjeldahl, J., 1883. Neue Methode zur Bestimmung des Stickstoffs in organischen. *J. Anal. Chem.* 366–382. <http://dx.doi.org/10.1007/BF01338151>.
- Kokaly, R., 1999. Spectroscopic determination of leaf biochemistry using band-depth analysis of absorption features and stepwise multiple linear regression. *Remote Sens. Environ.* 67, 267–287. [http://dx.doi.org/10.1016/S0034-4257\(98\)00084-4](http://dx.doi.org/10.1016/S0034-4257(98)00084-4).
- Lemaire, G., Jeuffroy, M.-H., Gastal, F., 2008. Diagnosis tool for plant and crop N status in vegetative stage: theory and practices for crop N management. *Eur. J. Agron.* 28, 614–624. <http://dx.doi.org/10.1016/j.eja.2008.01.005>.
- Li, P., Wang, Q., 2011. Retrieval of leaf biochemical parameters using PROSPECT inversion: a new approach for alleviating ill-posed problems. *IEEE Trans. Geosci. Remote Sens.* 49, 2499–2506. <http://dx.doi.org/10.1109/TGRS.2011.2109390>.
- Li, F., Mistele, B., Hu, Y., Chen, X., Schmidhalter, U., 2014. Reflectance estimation of canopy nitrogen content in winter wheat using optimised hyperspectral spectral indices and partial least squares regression. *Eur. J. Agron.* 52, 198–209. <http://dx.doi.org/10.1016/j.eja.2013.09.006>.
- Lichtenthaler, H.K., Lang, M., Sowinska, M., Heisel, F., Miehe, J.A., 1996. Detection of vegetation stress via a new high resolution fluorescence imaging system. *J. Plant Physiol.* 148, 599–612. [http://dx.doi.org/10.1016/S0176-1617\(96\)80081-2](http://dx.doi.org/10.1016/S0176-1617(96)80081-2).
- Lu, C., Zhang, J., 2000. Photosynthetic CO₂ assimilation, chlorophyll fluorescence and photoinhibition as affected by nitrogen deficiency in maize plants. *Plant Sci.* 151, 135–143.
- Mahajan, G.R., Sahoo, R.N., Pandey, R.N., Gupta, V.K., Kumar, D., 2014. Using hyperspectral remote sensing techniques to monitor nitrogen, phosphorus, sulphur and potassium in wheat (*Triticum aestivum* L.). *Precis. Agric.* 15, 499–522. <http://dx.doi.org/10.1007/s11119-014-9348-7>.
- Mahajan, G.R., Pandey, R.N., Sahoo, R.N., Gupta, V.K., Datta, S.C., Kumar, D., 2016. Monitoring nitrogen, phosphorus and sulphur in hybrid rice (*Oryza sativa* L.) using hyperspectral remote sensing. *Precis. Agric.* 1–26. <http://dx.doi.org/10.1007/s11119-016-9485-2>.
- Meroni, M., Busetto, L., Colombo, R., Guanter, L., Moreno, J., Verhoef, W., 2010. Performance of Spectral Fitting Methods for vegetation fluorescence quantification. *Remote Sens. Environ.* 114, 363–374. <http://dx.doi.org/10.1016/j.rse.2009.09.010>.
- Moya, I., Camenen, L., Evain, S., Goulas, Y., Cerovic, Z.G., Latouche, G., Flexas, J., Onis, A., 2004. A new instrument for passive remote sensing: 1. Measurements of sunlight-induced chlorophyll fluorescence. *Remote Sens. Environ.* 91, 186–197. <http://dx.doi.org/10.1016/j.rse.2004.02.012>.
- Nobel, P.S., 2009. Photochemistry of photosynthesis. *Physicochem. Environ. Plant Physiol.* 229–275. <http://dx.doi.org/10.1016/B978-0-12-374143-1.00005-3>.
- Pimstein, A., Karnieli, A., Bansal, S.K., Bonfil, D.J., 2011. Exploring remotely sensed technologies for monitoring wheat potassium and phosphorus using field spectroscopy. *Field Crops Res.* 121, 125–135. <http://dx.doi.org/10.1016/j.fcr.2010.12.001>.
- Plascyk, J.A., Gabriel, F.C., 1975. The Fraunhofer line discriminator MKII an airborne instrument for precise and standardized ecological luminescence measurement. *IEEE Trans. Instrum. Meas.* 24, 306–313. <http://dx.doi.org/10.1109/TIM.1975.4314448>.
- Quemada, M., Gabriel, J.L., Zarco-Tejada, P., 2014. Airborne hyperspectral images and ground-level optical sensors as assessment tools for maize nitrogen fertilization. *Remote Sens.* 6, 2940–2962. <http://dx.doi.org/10.3390/rs6042940>.
- R Core Team, 2015. R: A Language and Environment for Statistical Computing. R Foundation for Statistical Computing, Vienna, Austria. <http://www.R-project.org/>.
- Ranjan, R., Chopra, U.K., Sahoo, R.N., Singh, A.K., Pradhan, S., 2012. Assessment of plant nitrogen stress in wheat (*Triticum aestivum* L.) through hyperspectral indices. *Int. J. Remote Sens.* 33, 6342–6360. <http://dx.doi.org/10.1080/01431161.2012.687473>.
- Rascher, U., Alonso, L., Burkart, A., Cilia, C., Cogliati, S., Colombo, R., Damm, A., Drusch, M., Guanter, L., Hanus, J., Hyvärinen, T., Julitta, T., Jussila, J., Kataja, K., Kokkalis, P., Kraft, S., Kraska, T., Matveeva, M., Moreno, J., Muller, O., Panigada, C., Pisk, M., Pinto, F., Prey, L., Pude, R., Rossini, M., Schickling, A., Schurr, U., Schüttemeyer, D., Verrelst, J., Zemek, F., 2015. Sun-induced fluorescence – a new probe of photosynthesis: first maps from the imaging spectrometer HyPlant. *Glob. Chang. Biol.* 21, 4673–4684. <http://dx.doi.org/10.1111/gcb.13017>.
- Ravier, C., Quemada, M., Jeuffroy, M.-H., 2017. Use of a chlorophyll meter to assess nitrogen nutrition index during the growth cycle in winter wheat. *Field Crops Res.* 214, 73–82. <http://dx.doi.org/10.1016/j.fcr.2017.08.023>.
- Rondeaux, G., Steven, M., Baret, F., 1996. Optimization of soil-adjusted vegetation indices. *Remote Sens. Environ.* 55, 95–107. [http://dx.doi.org/10.1016/0034-4257\(95\)00186-7](http://dx.doi.org/10.1016/0034-4257(95)00186-7).
- Roujean, J.L., Breon, F.M., 1995. Estimating PAR absorbed by vegetation from bidirectional reflectance measurements. *Remote Sens. Environ.* 51, 375–384. [http://dx.doi.org/10.1016/0034-4257\(94\)00114-3](http://dx.doi.org/10.1016/0034-4257(94)00114-3).
- Rouse, J.W., Hass, R.H., Schell, J.A., Deering, D.W., 1973. Monitoring vegetation systems in the great plains with ERTS. *Third Earth Resour. Technol. Satell. Symp.* 1, 309–317 (citeulike-article-id:12009708).
- Sadras, V.O., 2004. Yield and water-use efficiency of water- and nitrogen-stressed wheat crops increase with degree of co-limitation. *Eur. J. Agron.* 21, 455–464. <http://dx.doi.org/10.1016/j.eja.2004.07.007>.
- Schächtl, J., Huber, G., Mair, F.-X., Sticksel, E., Schulz, J., Haschberger, P., 2005. Laser-Induced chlorophyll fluorescence measurements for detecting the nitrogen status of wheat (*Triticum aestivum* L.) canopies. *Precis. Agric.* 6, 143–156. <http://dx.doi.org/10.1007/s11119-004-1031-y>.
- Schlerf, M., Atzberger, C., 2006. Inversion of a forest reflectance model to estimate structural canopy variables from hyperspectral remote sensing data. *Remote Sens. Environ.* 100, 281–294. <http://dx.doi.org/10.1016/j.rse.2005.10.006>.
- Serrano, L., Penuelas, J., Ustin, S.L., 2002. Remote sensing of nitrogen and lignin in Mediterranean vegetation from AVIRIS data: decomposing biochemical from structural signals. *Remote Sens. Environ.* 81, 355–364.
- Smith, G.M., Milton, E.J., 1999. The use of the empirical line method to calibrate remotely sensed data to reflectance. *Int. J. Remote Sens.* 20, 2653–2662. <http://dx.doi.org/10.1080/014311699211994>.
- Stroppiana, D., Boschetti, M., Brivio, P.A., Bocchi, S., 2009. Plant nitrogen concentration in paddy rice from field canopy hyperspectral radiometry. *Field Crops Res.* 111, 119–129. <http://dx.doi.org/10.1016/j.fcr.2008.11.004>.
- Thorp, K.R., Wang, G., West, A.L., Moran, M.S., Bronson, K.F., White, J.W., Mon, J., 2012. Estimating crop biophysical properties from remote sensing data by inverting linked radiative transfer and ecophysiological models. *Remote Sens. Environ.* 124, 224–233. <http://dx.doi.org/10.1016/j.rse.2012.05.013>.
- Tremblay, N., Wang, Z., Cerovic, Z.G., 2012. Sensing crop nitrogen status with fluorescence indicators. A review. *Agron. Sustain. Dev.* 32, 451–464. <http://dx.doi.org/10.1007/s13593-011-0041-1>.
- Uddling, J., Gelang-Alfredsson, J., Piikki, K., Pleijel, H., 2007. Evaluating the relationship between leaf chlorophyll concentration and SPAD-502 chlorophyll meter readings. *Photosynth. Res.* 91, 37–46. <http://dx.doi.org/10.1007/s11120-006-9077-5>.
- Vogelmann, J.E., Rock, B.N., Moss, D.M., 1993. Red edge spectral measurements from sugar maple leaves. *Int. J. Remote Sens.* 14, 1563–1575. <http://dx.doi.org/10.1080/01431169308953986>.
- Walker, A.P., Beckerman, A.P., Gu, L., Kattge, J., Cernusak, L.A., Domingues, T.F., Scales, J.C., Wohlfahrt, G., Wullschlegel, S.D., Woodward, F.I., 2014. The relationship of leaf photosynthetic traits – V_{cmax} and J_{max} – to leaf nitrogen, leaf phosphorus, and specific leaf area: a meta-analysis and modeling study. *Ecol. Evol.* 4, 3218–3235. <http://dx.doi.org/10.1002/ece3.1173>.
- Wang, Y., Li, X., Nashed, Z., Zhao, F., Yang, H., Guan, Y., Zhang, H., 2007. Regularized kernel-based BRDF model inversion method for ill-posed land surface parameter retrieval. *Remote Sens. Environ.* 111, 36–50. <http://dx.doi.org/10.1016/j.rse.2007.03.007>.
- Wang, W., Yao, X., Yao, X., Tian, Y., Liu, X., Ni, J., Cao, W., Zhu, Y., 2012. Estimating leaf nitrogen concentration with three-band vegetation indices in rice and wheat. *Field Crops Res.* 129, 90–98. <http://dx.doi.org/10.1016/j.fcr.2012.01.014>.
- Wang, Z., Skidmore, A.K., Darvishzadeh, R., Heiden, U., Heurich, M., Wang, T., 2015. Leaf nitrogen content indirectly estimated by leaf traits derived from the PROSPECT model. *IEEE J. Sel. Top. Appl. Earth Obs. Remote Sens.* 8, 3172–3182. <http://dx.doi.org/10.1109/JSTARS.2015.2422734>.
- Weis, E., Berry, J.A., 1987. Quantum efficiency of Photosystem II in relation to energy-dependent quenching of chlorophyll fluorescence. *BBA Bioenergy* 894, 198–208. [http://dx.doi.org/10.1016/0005-2728\(87\)90190-3](http://dx.doi.org/10.1016/0005-2728(87)90190-3).
- Yang, X., Tang, J., Mustard, J.F., Lee, J., Rossini, M., Rascher, U., Alonso, L., Burkart, A., Cilia, C., Cogliati, S., Colombo, R., Damm, A., Drusch, M., Guanter, L., Hanus, J., Hyvärinen, T., Julitta, T., Jussila, J., Kataja, K., Kokkalis, P., Kraft, S., Kraska, T., Matveeva, M., Moreno, J., Muller, O., Panigada, C., Pisk, M., Pinto, F., Prey, L., Pude, R., Rossini, M., Schickling, A., Schurr, U., Schüttemeyer, D., Verrelst, J., Zemek, F., Houborg, R., Cescatti, A., Migliavacca, M., Kustas, W.P., Genty, B., Briantais, J.M., Baker, N.R., 2015. Satellite retrievals of leaf chlorophyll and photosynthetic capacity for improved modeling of GPP. *Agric. For. Meteorol.* 990, 10–23. <http://dx.doi.org/10.1111/gcb.13017>.
- Yebara, M., Chuvieco, E., 2009. Linking ecological information and radiative transfer

- models to estimate fuel moisture content in the Mediterranean region of Spain: solving the ill-posed inverse problem. *Remote Sens. Environ.* 113, 2403–2411. <http://dx.doi.org/10.1016/j.rse.2009.07.001>.
- Zarco-Tejada, P.J., Miller, J.R., Noland, T.L., Mohammed, G.H., Sampson, P.H., 2001. Scaling-up and model inversion methods with narrowband optical indices for chlorophyll content estimation in closed forest canopies with hyperspectral data. *IEEE Trans. Geosci. Remote Sens.* 39, 1491–1507. <http://dx.doi.org/10.1109/36.934080>.
- Zarco-Tejada, P.J., Berjon, A., Miller, J.R., 2004. Stress detection in crops with hyperspectral remote sensing and physical simulation models. *Airborne Imaging Spectrosc. Work* 1–5.
- Zarco-Tejada, P.J., Berjón, A., López-Lozano, R., Miller, J.R., Martín, P., Cachorro, V., González, M.R., De Frutos, A., 2005. Assessing vineyard condition with hyperspectral indices: leaf and canopy reflectance simulation in a row-structured discontinuous canopy. *Remote Sens. Environ.* 99, 271–287. <http://dx.doi.org/10.1016/j.rse.2005.09.002>.
- Zarco-Tejada, P.J., González-Dugo, V., Berni, J.A.J., 2012. Fluorescence, temperature and narrow-band indices acquired from a UAV platform for water stress detection using a micro-hyperspectral imager and a thermal camera. *Remote Sens. Environ.* 117, 322–337. <http://dx.doi.org/10.1016/j.rse.2011.10.007>.
- Zarco-Tejada, P.J., Catalina, A., González, M.R., Martín, P., 2013. Relationships between net photosynthesis and steady-state chlorophyll fluorescence retrieved from airborne hyperspectral imagery. *Remote Sens. Environ.* 136, 247–258. <http://dx.doi.org/10.1016/j.rse.2013.05.011>.
- Zarco-Tejada, P.J., González-Dugo, M.V., Fereres, E., 2016. Seasonal stability of chlorophyll fluorescence quantified from airborne hyperspectral imagery as an indicator of net photosynthesis in the context of precision agriculture. *Remote Sens. Environ.* 179, 89–103. <http://dx.doi.org/10.1016/j.rse.2016.03.024>.